

Synchronization of flexible sheets

GWYNN J. ELFRING AND ERIC LAUGA†

Department of Mechanical and Aerospace Engineering, University of California San Diego,
9500 Gilman Drive, La Jolla, CA 92093-0411, USA

(Received 30 November 2010; revised 27 January 2011; accepted 13 February 2011;
first published online 22 March 2011)

When swimming in close proximity, some microorganisms such as spermatozoa synchronize their flagella. Previous work on swimming sheets showed that such synchronization requires a geometrical asymmetry in the flagellar waveforms. Here we inquire about a physical mechanism responsible for such symmetry breaking in nature. Using a two-dimensional model, we demonstrate that flexible sheets with symmetric internal forcing deform when interacting with each other via a thin fluid layer in such a way as to systematically break the overall waveform symmetry, thereby always evolving to an in-phase conformation where energy dissipation is minimized. This dynamics is shown to be mathematically equivalent to that obtained for prescribed waveforms in viscoelastic fluids, emphasizing the crucial role of elasticity in symmetry breaking and synchronization.

Key words: biological fluid dynamics, low-Reynolds-number flows, micro-organism dynamics

1. Introduction

Motile microorganisms swim in a fluid regime where inertia is unimportant and viscous stresses dominate. In this limit the flow field due to a swimmer affects the motility of nearby cells (Lauga & Powers 2009), a fact which is biologically important as microorganisms such as spermatozoa are often found in high-density suspensions (Suarez & Pacey 2006). A particular consequence of these fluid-based interactions is the synchronization of the flagella of some spermatozoa observed to occur when these cells are swimming in close proximity (Hayashi 1998; Riedel, Kruse & Howard 2005; Woolley *et al.* 2009).

Taylor (1951) provided the first quantitative analysis of this phenomenon in his landmark work on the mechanics of swimming microorganisms. Using a two-dimensional model of sheets passing sinusoidal waves of transverse displacement, he showed that the energy dissipated by the fluid due to such motions, for two swimmers a fixed distance apart, is minimized if they are in-phase (Taylor 1951). Subsequent computational studies (Fauci 1990; Fauci & McDonald 1995; Yang, Elgeti & Gompper 2008) have shown that such synchronization can occur due to fluid forces alone.

In recent theoretical analysis it was demonstrated that two infinite sheets passing waves of a prescribed shape will not synchronize in a Newtonian fluid if the shape of the waveforms η_1 and η_2 satisfy $\eta_2(x) = -\eta_1(-x + \theta)$ (where θ is a fixed phase shift and x is the direction along the sheets) because of the kinematic reversibility

† Email address for correspondence: elauga@ucsd.edu

of the Stokes equations (Elfring & Lauga 2009, 2011). The sinusoidal waveforms of Taylor's swimming sheet clearly fall into this category, and will thus not dynamically synchronize in a Newtonian fluid. It has been observed that excess symmetry similarly curbs synchronization in other models (Kim & Powers 2004; Pooley, Alexander & Yeomans 2007; Putz & Yeomans 2009; Golestanian, Yeomans & Uchida 2011; Uchida & Golestanian 2011). For a sinusoidal sheet, a geometric perturbation must, therefore, be added (for example in the form of a higher order mode) to break the necessary front/back symmetry and to give rise to a time evolution of phase towards the synchronized state (Elfring & Lauga 2009, 2011). Alternatively, instead of a geometric symmetry breaking, it has also been shown that synchronization can occur if the kinematic reversibility of the field equations is removed, as is the case for a viscoelastic fluid (Elfring, Pak & Lauga 2010). In such a scenario the phase always evolves to a stable in-phase conformation where the energy dissipated by the swimmers is minimized.

In this paper we inquire about a physical mechanism responsible for symmetry breaking in real biological cells. Instead of delineating a fixed waveform for the swimming sheets, we take the more realistic modelling approach of passing internal waves of bending as produced by a flagellum's internal structure (or axoneme) (Riedel-Kruse *et al.* 2007). In the case of a single sheet, similar models have been employed to study swimming (Argentina, Skotheim & Mahadevan 2007; Balmforth, Coombs & Pachmann 2010) and peeling (Hosoi & Mahadevan 2004). We use this model to show that elastic deformation due to fluid body interactions, with purely sinusoidal forcing, always leads to in-phase synchronization.

Flexibility has long been considered as an avenue for symmetry breaking in Stokes flow. Purcell, in his celebrated talk and paper (Purcell 1977), asserted that while a stiff oar undergoing reciprocal motion would produce no net motion, due to the scallop theorem, a flexible oar would escape this conundrum because of a broken symmetry between forward and reverse strokes. This was first investigated analytically by Machin (1958), while more recently a number of theoretical and experimental studies have further elucidated the effect of flexibility quantitatively, both for boundary-driven (Wiggins & Goldstein 1998; Yu, Lauga & Hosoi 2006; Lauga 2007) and internally driven filaments (Camalet, Jülicher & Prost 1999; Camalet & Jülicher 2000; Dreyfus *et al.* 2005).

Recently, the analysis of a pair rotating helices as a model for bacterial flagella has shown flexibility to be a crucial ingredient for synchronization (Reichert & Stark 2005), as was similarly shown for a minimal model of interacting cilia (Niedermayer, Eckhardt & Lenz 2008). Additionally, flexibility has been found to be requisite for the synchronization of paddles that would otherwise be too symmetric to yield stable fixed points (Qian *et al.* 2009). In these models and experiments, the bodies are rigid, but permitted to deviate from their trajectories, in an elastic manner in response to fluid forces. In contrast, here we allow the bodies themselves to deform due to fluid stresses induced by the other swimmer.

Our approach is organized as follows. For a pair of two-dimensional sheets in the lubrication limit, we derive a system of nonlinear equations governing both the fluid stresses and the resulting swimmer shapes. We linearize these equations to produce analytical solutions, and then solve the nonlinear equations numerically. We show that flexible sheets with symmetric sinusoidal forcing will deform when interacting with each other via a thin fluid layer in such a way as to break geometrical symmetry, and to evolve to an in-phase conformation where energy dissipation is minimized. Further, this evolution of phase is shown to be functionally equivalent to that found

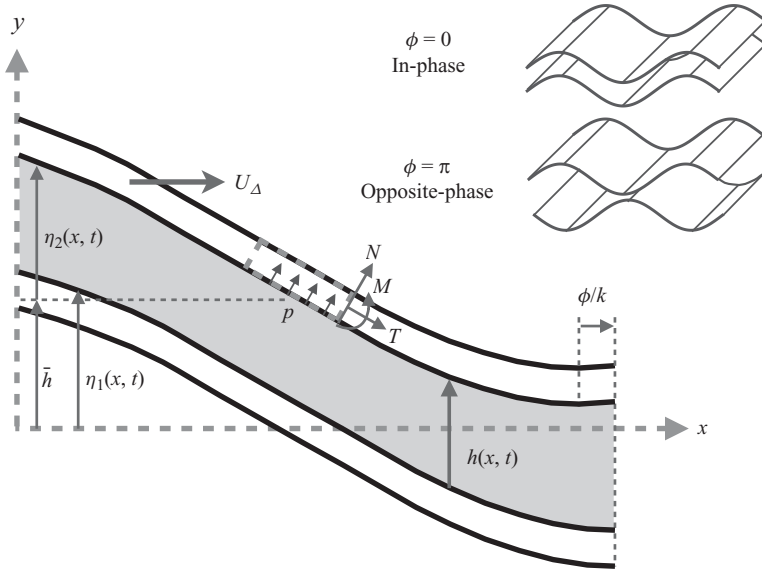


FIGURE 1. System of two infinite two-dimensional sheets, of shape described by the functions η_1 and η_2 , which are separated by a fluid layer of thickness h (mean value, \bar{h}), have a relative phase ϕ and may move relative to each other with a velocity U_Δ . An infinitesimal material element on the top sheet is subject to fluid pressure p , normal force N , tension T and moment M . Inset: schematic representation of in-phase and opposite-phase configurations.

for prescribed waveforms in viscoelastic fluids (Elfring *et al.* 2010), illuminating the role of elasticity in symmetry breaking and synchronization.

2. Model system

We consider the dynamics of two infinite two-dimensional elastic sheets which are separated by a fluid layer of mean distance \bar{h} (see figure 1). The sheets deform due to a balance between an active moment m , passive bending (elastic) resistance and fluid stresses. The positions of the sheets are given by $y_1 = \eta_1(x, t)$ for the bottom sheet and $y_2 = \bar{h} + \eta_2(x, t)$ for the top sheet. We look to solve this problem in the limit that the fluid layer is thin compared to the wavelength of the sheets, $k\bar{h} \ll 1$, to make use of Reynolds' lubrication approximation for the fluid field equations (Reynolds 1886).

An infinitesimal element along one sheet is subject to tension, T , normal force, N , and moment, M (shown in figure 1). Since the fluid layer is thin and lubrication forces are singular with the gap thickness, forces from the outer flow are safely ignored (Balmforth *et al.* 2010). To capture the active bending of the sheet we use a model for the flagella of eukaryotes introduced by Jülicher and co-workers (Camalet & Jülicher 2000; Riedel-Kruse *et al.* 2007) where the bending of an elastic filament (flagellum) is caused by the constrained sliding of microtubule doublets; the effect of the internal forces which induce sliding is here represented by an active moment density m . Given that we are in an overdamped limit we take the equilibrium shapes to arise instantaneously (Hosoi & Mahadevan 2004). Assuming reasonably small deflections such that the swimmers are linearly elastic (Landau & Lifshitz 1986), force (F) and moment (M) balance on the top sheet yield, respectively:

$$\frac{\partial F}{\partial x} = -\mathbf{n} \cdot \boldsymbol{\sigma}, \quad \frac{\partial M}{\partial x} = -N + m, \quad (2.1)$$

where \mathbf{n} is the unit normal and $\boldsymbol{\sigma}$ is the fluid stress tensor. The relation between the moment and the sheet curvature is given by the constitutive relation $M = B\partial^2\eta/\partial x^2$, where B is the sheet bending stiffness. Combining with (2.1) we obtain the equations governing the shape of the sheets:

$$B\frac{\partial^4\eta}{\partial x^4} = \frac{\partial m}{\partial x} \mp \mathbf{n} \cdot \boldsymbol{\sigma} \cdot \mathbf{n}, \quad (2.2)$$

where \mp are for the top and bottom sheets, respectively. If resistive force theory is used for the fluid forces then we obtain the governing equation used by Riedel-Kruse *et al.* (2007) for a single filament.

The internal forcing on the sheets is assumed to take the form $m(x, t) = Ag(kx - ckt)$, where k is the wavenumber, c is the wave speed, A is the amplitude of the moment and g is an arbitrary but 2π -periodic function. Because the forcing is periodic, we will assume the shape η to be also periodic. We non-dimensionalize vertical distances by $y^* = y/\bar{h}$ and horizontal distances by $x^* = kx$ (* indicates a dimensionless quantity). Non-dimensionalizing the continuity equation, we find that if the horizontal velocity is given by $u = cu^*$ then the vertical velocity must be $v = \epsilon cv^*$, where $\epsilon = k\bar{h}$. The Stokes equations then yield the lubrication equations to leading order in ϵ :

$$\frac{\partial p^*}{\partial x^*} = \frac{\partial^2 u^*}{\partial y^{*2}}, \quad \frac{\partial p^*}{\partial y^*} = 0, \quad (2.3)$$

$$\frac{\partial u^*}{\partial x^*} + \frac{\partial v^*}{\partial y^*} = 0, \quad (2.4)$$

where $p^* = \epsilon^2 p/\mu\omega$. Forces (per unit depth) are non-dimensionalized as $f^* = f\epsilon/\mu c$, while energy dissipation rate per unit depth is $\dot{E}^* = \epsilon^2 \dot{E}/\mu\omega c\bar{h}$.

In the lubrication limit, $\epsilon \ll 1$, the normal force due to the fluid on the beam is to leading order merely the pressure, $-\mathbf{n} \cdot \boldsymbol{\sigma} \cdot \mathbf{n} = p$. Since the field equations for the fluid yield the pressure gradient, we differentiate (2.2), and recasting the equation in dimensionless form we obtain

$$B^* \frac{\partial^5 \eta^*}{\partial x^{*5}} = A^* \frac{\partial^2 g}{\partial x^{*2}} \pm \frac{dp^*}{dx^*}, \quad (2.5)$$

where $B^* = B\epsilon^3 k^3/\mu\omega$ is the dimensionless bending stiffness and $A^* = A\epsilon^2 k^2/\mu\omega$ is the dimensionless amplitude of the active bending moment. This equation allows us to solve for the shape of the sheets, $\eta_{1,2}$, and is coupled to the fluid field equations through the pressure gradient. We now drop the * for convenience.

3. Analysis

Given the form of the forcing we expect post-transient solutions which are functions of a wave variable $z = x - t$ and thus we write $\eta = \eta(z)$. The top sheet may move relative to the bottom sheet with a horizontal velocity $u = U_\Delta$, hence the boundary conditions for the fluid equations (2.4), in a frame moving with waveform, are given by $u(x, y_1) = -1$, $v(x, y_1) = -\eta'_1$, $u(x, y_2) = U_\Delta - 1$ and $v(x, y_2) = -\eta'_2$. Given the above boundary conditions the solution for the velocity field is found to be

$$u(x, y) = \frac{1}{2} \frac{dp}{dx} (y - y_1)(y - y_2) + U_\Delta \frac{y - y_1}{y_2 - y_1} - 1. \quad (3.1)$$

If one integrates the continuity equation one finds

$$\frac{\partial}{\partial x} \int_{y_1}^{y_2} u \, dy = U_{\Delta} \frac{d\eta_2}{dx}. \quad (3.2)$$

If $U_{\Delta} = 0$ then the flow rate between the sheets is constant. Integrating (3.2) and exploiting the periodicity of the pressure (Elfring & Lauga 2009), we obtain the equation for the pressure gradient as

$$\frac{dp}{dx} = \frac{6U_{\Delta} - 12}{h^2} - \frac{12U_{\Delta}y_2}{h^3} - \frac{(6U_{\Delta} - 12)I_2 - 12U_{\Delta}J_3}{I_3h^3}, \quad (3.3)$$

where the distance between the two sheets is given by $h = 1 + \eta_2 - \eta_1$ and $I_j = \int_0^{2\pi} h^{-j} dx$ and $J_3 = \int_0^{2\pi} y_2 h^{-3} dx$. Then the force on the top sheet is given by

$$f_x = \int_0^{2\pi} \left(y_2 \frac{dp}{dx} - \frac{\partial u}{\partial y} \right) \Big|_{y=y_2} dx = \int_0^{2\pi} \left[\frac{1}{2} \frac{dp}{dx} (\eta_2 + \eta_1) - \frac{U_{\Delta}}{1 + \eta_2 - \eta_1} \right] dx. \quad (3.4)$$

3.1. Linear regime: statics

We first look at the case where we enforce $U_{\Delta} = 0$ (i.e. we fix the top sheet with respect to the bottom sheet) in order to determine under which condition a non-zero synchronization force will arise.

If we assume the dimensionless amplitude of the forcing A to be small, and the dimensionless bending stiffness B to be large, then the shape amplitude (or maximum value of the shape) $\|\eta\|_{\infty}$ is expected to be also small. Linearizing the pressure gradient for small η , with $U_{\Delta} = 0$ gives

$$\frac{dp}{dx} \approx -12(\eta_2 - \eta_1), \quad (3.5)$$

where we have invoked an integrated conservation of mass, $\langle \eta_2 - \eta_1 \rangle = 0$ (angle brackets $\langle \rangle$ denote the average over a period). Our goal now is to determine whether two sheets which are equally and symmetrically forced but with a phase shift ϕ will synchronize in time. With this in mind we let $g_2 = g_1(z + \phi)$ with $g_1(z) = \cos(z)$, and we set equal for both sheets the bending stiffness B and the forcing amplitude A . The linearized governing equations are then given by

$$B \frac{d^5 \eta_1}{dz^5} - 12(\eta_2 - \eta_1) = -A \cos(z), \quad (3.6a)$$

$$B \frac{d^5 \eta_2}{dz^5} + 12(\eta_2 - \eta_1) = -A \cos(z + \phi). \quad (3.6b)$$

To solve these equations we apply periodic boundary conditions. The solution of this system of equations with the linearized pressure gradient (3.5) can be found analytically to be

$$\eta_1(z) = A \frac{12B [\cos(z + \phi) - \cos z] - [(288 + B^2) \sin z + 288 \sin(z + \phi)]}{B(576 + B^2)} + C, \quad (3.7a)$$

$$\eta_2(z) = A \frac{12B [\cos z - \cos(z + \phi)] - [288 \sin z + (288 + B^2) \sin(z + \phi)]}{B(576 + B^2)} + C. \quad (3.7b)$$

Note that nothing prevents the solution from including a uniform shift $C(A, B)$; however, the relevant physics of the problem are invariant under such a shift and hence the value of C is irrelevant (equivalently, we place our z -axis at $\langle \eta_1 \rangle = 0$).

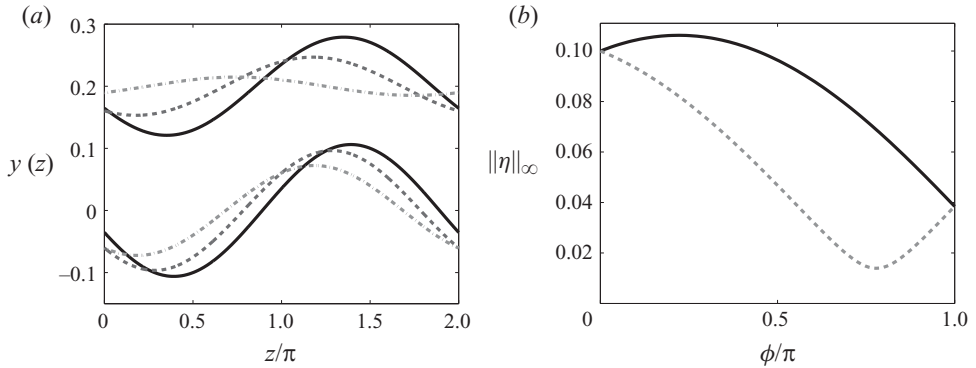


FIGURE 2. (a) Solution shapes, (3.7), for various phase differences $\phi = \pi/4$ (solid lines), $\pi/2$ (dashed lines) and $3\pi/4$ (dashed-dotted lines), with $A=1$ and $B=10$. We observe that the amplitude is not evenly affected by the pressure (the plot is shown here with $\bar{h}=0.2$ rather than $\bar{h}=1$ for display purposes only). (b) Shape amplitude, $\|\eta\|_\infty$, versus phase difference, ϕ (bottom sheet: solid line; top sheet: dashed line). Lines are reversed upon the change $\phi \rightarrow -\phi$.

Both shapes in (3.7) are delineated by the competition between bending rigidity, the pressure gradient in the fluid and the internal forcing (with ϕ dependence). In this linear limit we note that the sheets are linear in the forcing amplitude A , and when $A=0$ then as expected they become straight, i.e. $\eta=0$. In the limit where rigidity dominates, $B \rightarrow \infty$, then the sheets also tend to become straight, $\eta \rightarrow 0$. If the rigidity and forcing amplitude are both very large ($A, B \gg 1$) then we can scale out the contribution from the fluid forces in (3.6) and we are left with $\eta_1 \approx -(A/B) \sin z$ and $\eta_2 \approx -(A/B) \sin(z + \phi)$ as might be expected. Note finally that the solutions in (3.7) are only valid when $B \gg A$ as otherwise unphysical solutions may arise with the sheets overlapping; this is prevented when the full nonlinear form of the pressure gradient is kept, as it diverges when $h \rightarrow 0$.

Solutions to (3.7) for $A=1$, $B=10$ and three values of the phase difference ($\phi = \pi/4, \pi/2, 3\pi/4$) are plotted in figure 2(a). We observe that the shapes are sinusoidal and hence individually remain symmetric both about the vertical axis and the horizontal axis. The global asymmetry that arises, however, is that the amplitudes of the two waveforms are not equally modulated by the fluid pressure, as shown in figure 2(b). We see that the top sheet indeed has a smaller amplitude for positive ϕ (and by symmetry, this is reversed upon changing $\phi \rightarrow -\phi$).

The phase locking force on the top sheet is, at leading order, given by

$$f_x = -6 \int_0^{2\pi} (\eta_2 - \eta_1)(\eta_2 + \eta_1) dx = 2\pi\alpha \sin \phi, \quad (3.8)$$

where $\alpha = 144A^2/(576B + B^3)$. Equation (3.8) is the main result of our paper. The phase locking force is proportional to the sine of the phase, meaning that the only stable fixed point occurs at $\phi=0$, and hence all initial conformations will evolve to the stable in-phase conformation. We, thus, see that the elasticity of the swimmers and fluid-structure interactions, can introduce the geometrical symmetry breaking necessary to develop a non-zero phase locking force. The force is found to be quadratic in amplitude, reminiscent of viscoelastic symmetry breaking (Elfring *et al.* 2010); by comparison, the phase-locking force arises at fourth order in amplitude for prescribed and identical asymmetric waveforms in a Newtonian fluid. The reason for the difference is that with elastic deformation the sheets are ultimately not the

same shape, despite having identical mechanical properties, and hence $\langle \eta_1^2 \rangle \neq \langle \eta_2^2 \rangle$; for prescribed waveforms this is different as the same waveform is prescribed for both sheets, and the quadratic term of the force vanishes.

The energy dissipated by the fluid between the two swimming cells to leading order is

$$\dot{E} = 12 \int_0^{2\pi} (\eta_2 - \eta_1)^2 dx = \frac{24\pi A^2}{576 + B^2} (1 - \cos \phi). \quad (3.9)$$

We see that the energy dissipation is a global minimum when $\phi = 0$ and global maximum when $\phi = \pi$. It follows then that the cells will always evolve to a state of minimum energy dissipation. We observe that the form of the energy dissipation is precisely the same as that for fixed shapes (and taking the fixed wave amplitude $A_{fixed}^2 = A^2/(576 + B^2)$ they are equal) (Elfring & Lauga 2011). It is important to note that waveforms with a prescribed broken symmetry may evolve to either the in-phase or opposite-phase conformation (Elfring & Lauga 2009); in contrast, the natural symmetry breaking due to elasticity of the bodies, or in the fluid, leads to a conformation of minimum energy dissipation.

3.2. Linear regime: dynamics

When the sheets are permitted to evolve in time in force-free swimming, the relative velocity U_Δ may be non-zero. In order to determine the leading order component of the pressure field we must first find out how the relative velocity scales with the sheet amplitudes. Given that the net force on the sheets in the dynamic case must now be zero, we obtain at leading order the relative speed as given by

$$U_\Delta = -\frac{3}{\pi} \int_0^{2\pi} (\eta_2 - \eta_1)(\eta_2 + \eta_1) dx. \quad (3.10)$$

We see that the velocity is quadratic in amplitude and is indeed proportional to the static force $U_\Delta = f_x^s/2\pi$ (we use here the superscript s to indicate the static force given by (3.8) to avoid confusion). With this we thus know that at leading order the pressure field (for a given ϕ) is invariant between the static and dynamic case, and since the beam equation couples via the pressure field, our instantaneous shapes are found to be the same. The only difference is that now the phase difference changes in time (geometrically) due to the presence of a non-zero relative velocity, according to $d\phi/dt = -U_\Delta$. Using (3.10), we find the rate of change of the phase at leading order to be given by

$$\frac{d\phi}{dt} = -\alpha \sin \phi. \quad (3.11)$$

Equation (3.11) can be integrated analytically, leading to a time evolution of the phase given by

$$\phi(t) = 2 \tan^{-1} \left[\tan \left(\frac{\phi_0}{2} \right) e^{-\alpha t} \right]. \quad (3.12)$$

All initial conformations, ϕ_0 , decay in time to the stable in-phase conformation, $\phi = 0$. Notably, the time evolution of the phase for a sinusoidally forced elastic sheet we obtain here is mathematically similar to that for a fixed sinusoidal waveform in a viscoelastic fluid (Elfring *et al.* 2010) and for rigid bodies with flexible trajectories (Niedermayer *et al.* 2008), emphasizing, therefore, the crucial role of elasticity in synchronization.

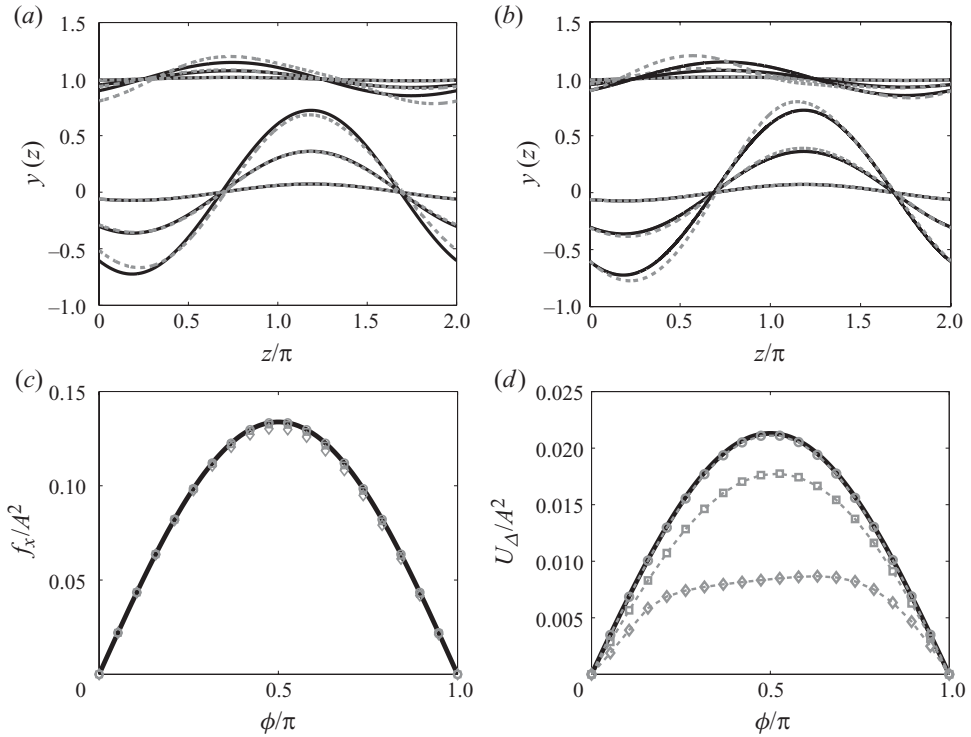


FIGURE 3. The solution shapes, η_1 and η_2 , for bending stiffness $B=10$, phase difference $\phi=3\pi/4$ and amplitudes $A=\{1, 5, 10\}$: (a) $U_\Delta=0$; (b) $f_x=0$); linearized pressure approximation: solid lines; full pressure gradient: dashed lines. (c) Phase locking force, f_x/A^2 , versus phase difference, ϕ , when $U_\Delta=0$; (d) relative velocity, U_Δ/A^2 , versus ϕ , when $f_x=0$. Both plots are for numerical solutions of the nonlinear equations with $B=10$ and $A=1$ (circles), 5 (squares) and 10 (diamonds); linearized solutions are shown as solid lines. Away from the linear regime, the rate of change of the phase is affected, while the forces are not.

Finally, if we allow a small difference in the wavespeeds of the sheets, $\Delta\omega$, then to leading order we have the same evolution of phase, (3.11) and (3.12), but now the rate of change of phase is defined as $\dot{\phi} = -U_\Delta - \Delta\omega$ and hence we see a synchronization of shape but not of material points.

3.3. Nonlinear case

To move beyond the linear regime, we now solve the nonlinear equations for the shapes (2.5) numerically, together with (3.3), using Matlab's boundary value problem solver `bvp4c`, both for the static case, $U_\Delta=0$, and the force-free case, $f_x=0$, using (3.4).

We find the linearized pressure gradient to be a capable approximation, particularly when the bending is of the same order as the pressure $B \sim 1$ and the phase difference is small; however, when $A, B \gg 1$ the linearized pressure may lead to unphysical solutions particularly if the sheets are near opposite-phase as the divergent nature of the full form of the pressure gradient is required to deform the sheets from contact.

In figure 3 we illustrate the breakdown of the linear regime. We plot the static shapes ($U_\Delta=0$, top left) and dynamic shapes ($f_x=0$, top right), both with a phase difference of $\phi=3\pi/4$, bending stiffness $B=10$ and with forcing amplitudes $A=\{1, 5, 10\}$. We see that for increasing amplitude the shapes predicted by linearized equations

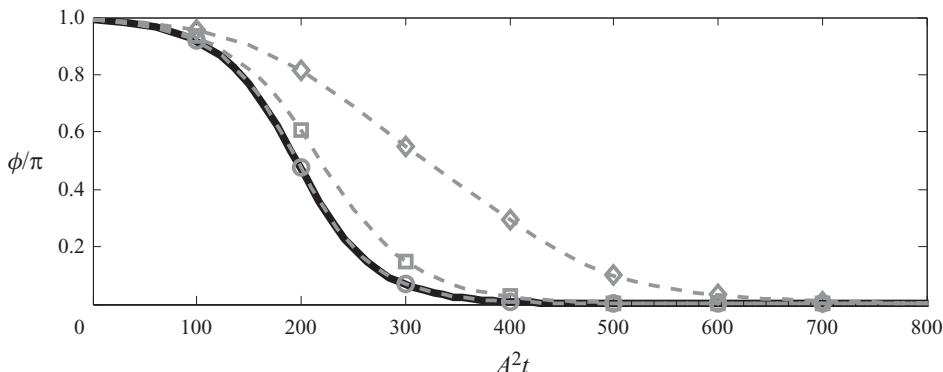


FIGURE 4. Time evolution of the phase difference, ϕ , in the nonlinear problem for $B = 10$ starting from an initial angle of $\phi/\pi = .99$ and with forcing amplitude $A = 1$ (circles), 5 (squares) and 10 (diamonds); the linear estimate is shown solid. As the forcing amplitude increases, the linear solution increasingly underestimates the time scale to synchronize.

(solid) and nonlinear equations (dashed) begin to diverge. In particular the nonlinear equations lead to a pronounced left–right asymmetry in the individual shape. In the lower left plot of figure 3 we display the phase locking force versus phase, while in the lower right plot we show the relative velocity versus phase, both with $B = 10$ and $A = \{1, 5, 10\}$ (circles, squares and diamonds, respectively) for the numerical solutions to the nonlinear equations; the analytical solutions for the linear equations are shown solid. The synchronizing hydrodynamic force, f_x , found by either method remains remarkably consistent even for very large forcing amplitude, A . In contrast, the rate of change of the phase decreases markedly from the linear approximation for large amplitude waves. Because the force is virtually unaffected, we, therefore, know that the resistance to motion is dramatically increased by the change in shape.

In figure 4 we integrate the instantaneous relative velocity to obtain the evolution of the phase in time. We show solution to both the linear equations (solid) and nonlinear equations (dashed) for $B = 10$ and $A = \{1, 5, 10\}$ starting from an initial phase difference of just less than π . We see that, as the forcing amplitude increases, the nonlinear equations yield an increasingly slower evolution to a synchronized conformation than that predicted by the linear regime; however, the general behaviour remains qualitatively unchanged.

4. Conclusion

In this paper we inquired about a physical mechanism responsible for symmetry breaking and synchronization in the flagella of biological cells such as spermatozoa. In a Newtonian fluid, two swimming sheets passing waveforms of a prescribed sinusoidal shape will not synchronize due to an excess of symmetry; however, here we have demonstrated that identical flexible sheets with symmetric sinusoidal forcing will deform, when interacting with each other via a thin fluid layer, in such a way as to systematically break the overall geometrical symmetry. This system will always evolve to an in-phase conformation where energy dissipation is minimized, in contrast to a prescribed asymmetry, which may maximize energy dissipation. In addition, this time evolution of the relative phase is shown to be equivalent to that obtained for prescribed waveforms in viscoelastic fluids (Elfring *et al.* 2010), emphasizing the

crucial role of elasticity in symmetry breaking and synchronization – be it that of the fluid or the swimmers themselves.

Funding by the NSF (CBET-0746285) and NSERC (PGS D3-374202) is gratefully acknowledged.

REFERENCES

- ARGENTINA, M., SKOTHEIM, J. & MAHADEVAN, L. 2007 Settling and swimming of flexible fluid-lubricated foils. *Phys. Rev. Lett.* **99**, 224503.
- BALMFORTH, N. J., COOMBS, D. & PACHMANN, S. 2010 Microelastohydrodynamics of swimming organisms near solid boundaries in complex fluids. *Q. J. Mech. Appl. Math.* **63**, 267–294.
- CAMALET, S. & JÜLICHER, F. 2000 Generic aspects of axonemal beating. *New J. Phys.* **2**, 24.
- CAMALET, S., JÜLICHER, F. & PROST, J. 1999 Self-organized beating and swimming of internally driven filaments. *Phys. Rev. Lett.* **82**, 1590–1593.
- DREYFUS, R., BAUDRY, J., ROPER, M. L., FERMIGIER, M., STONE, H. A. & BIBETTE, J. 2005 Microscopic artificial swimmers. *Nature* **437**, 862–865.
- ELFRING, G. J. & LAUGA, E. 2009 Hydrodynamic phase locking of swimming microorganisms. *Phys. Rev. Lett.* **103**, 088101.
- ELFRING, G. J. & LAUGA, E. 2011 Passive hydrodynamic synchronization of two-dimensional swimming cells. *Phys. Fluids* **23**, 011902.
- ELFRING, G. J., PAK, O. S. & LAUGA, E. 2010 Two-dimensional flagellar synchronization in viscoelastic fluids. *J. Fluid Mech.* **646**, 505–515.
- FAUCI, L. J. 1990 Interaction of oscillating filaments: a computational study. *J. Comput. Phys.* **86**, 294–313.
- FAUCI, L. J. & McDONALD, A. 1995 Sperm motility in the presence of boundaries. *Bull. Math. Biol.* **57**, 679–699.
- GOLESTANIAN, R., YEOMANS, J. M. & UCHIDA, N. 2011 Hydrodynamic synchronization at low Reynolds number. *Soft Matt.* (Advance Article, doi: 10.1039/C0SM01121E).
- HAYASHI, F. 1998 Sperm co-operation in the fishfly, *parachauliodes japonicus*. *Funct. Ecol.* **12**, 347–350.
- HOSOI, A. E. & MAHADEVAN, L. 2004 Peeling, healing, and bursting in a lubricated elastic sheet. *Phys. Rev. Lett.* **93**, 137802.
- KIM, M. & POWERS, T. R. 2004 Hydrodynamic interactions between rotating helices. *Phys. Rev. E* **69**, 061910.
- LANDAU, L. D. & LIFSHITZ, E. M. 1986 *Theory of Elasticity: Vol. 7 of Course of Theoretical Physics*. Butterworth-Heinemann.
- LAUGA, E. 2007 Propulsion in a viscoelastic fluid. *Phys. Fluids* **19**, 083104.
- LAUGA, E. & POWERS, T. R. 2009 The hydrodynamics of swimming microorganisms. *Rep. Prog. Phys.* **72**, 096601.
- MACHIN, K. E. 1958 Wave propagation along flagella. *J. Exp. Biol.* **35**, 796–806.
- NIEDERMAYER, T., ECKHARDT, B. & LENZ, P. 2008 Synchronization, phase locking, and metachronal wave formation in ciliary chains. *Chaos: An Interdisciplinary J. Nonlinear Sci.* **18**, 037128.
- POOLEY, C. M., ALEXANDER, G. P. & YEOMANS, J. M. 2007 Hydrodynamic interaction between two swimmers at low Reynolds number. *Phys. Rev. Lett.* **99**, 228103.
- PURCELL, E. M. 1977 Life at low Reynolds number. *Am. J. Phys.* **45**, 3–11.
- PUTZ, V. B. & YEOMANS, J. M. 2009 Hydrodynamic synchronisation of model microswimmers. *J. Stat. Phys.* **137**, 1001–1013 .
- QIAN, B., JIANG, H., GAGNON, D. A., BREUER, K. S. & POWERS, T. R. 2009 Minimal model for synchronization induced by hydrodynamic interactions. *Phys. Rev. E* **80**, 061919.
- REICHERT, M. & STARK, H. 2005 Synchronization of rotating helices by hydrodynamic interactions. *Eur. Phys. J. E* **17**, 493–500.
- REYNOLDS, O. 1886 On the theory of lubrication and its application to Mr. Beauchamp Tower's experiments, including an experimental determination of the viscosity of olive oil. *Phil. Trans. R. Soc. Lond.* **177**, 157–234.

- RIEDEL, I. H., KRUSE, K. & HOWARD, J. 2005 A self-organized vortex array of hydrodynamically entrained sperm cells. *Science* **309**, 300–303.
- RIEDEL-KRUSE, I. H., HILFINGER, A., HOWARD, J. & JÜLICHER, F. 2007 How molecular motors shape the flagellar beat. *HFSP J.* **1**, 192–208.
- SUAREZ, S. S. & PACEY, A. A. 2006 Sperm transport in the female reproductive tract. *Human Reprod. Update* **12**, 23–37.
- TAYLOR, G. I. 1951 Analysis of the swimming of microscopic organisms. *Proc. R. Soc. Lond. A* **209**, 447–461.
- UCHIDA, N. & GOLESTANIAN, R. 2011 Generic conditions for hydrodynamic synchronization. *Phys. Rev. Lett.* **106**, 058104.
- WIGGINS, C. H. & GOLDSTEIN, R. E. 1998 Flexive and propulsive dynamics of elastica at low Reynolds number. *Phys. Rev. Lett.* **80**, 3879–3882.
- WOOLLEY, D. M., CROCKETT, R. F., GROOM, W. D. I. & REVELL, S. G. 2009 A study of synchronisation between the flagella of bull spermatozoa, with related observations. *J. Exp. Biol.* **212**, 2215–2223.
- YANG, Y., ELGETI, J. & GOMPPER, G. 2008 Cooperation of sperm in two dimensions: synchronization, attraction, and aggregation through hydrodynamic interactions. *Phys. Rev. E* **78**, 061903.
- YU, T. S., LAUGA, E. & HOSOI, A. E. 2006 Experimental investigations of elastic tail propulsion at low Reynolds number. *Phys. Fluids* **18**, 091701.